Research Article Vol. 30, No. 12 / 6 Jun 2022 / Optics Express 22247
Optics EXPRESS

Active Fano resonance switch using dual-layer graphene in an embedded dielectric metasurface

DONGJUN SEO, JOON KI LEE, AND GYEONG CHEOL PARK*

Electronics and Telecommunications Research Institute, Daejeon 34129, Republic of Korea
*gcpark@etri.re.kr

Abstract: We propose an active optical Fano switch (OFS) based on an embedded dielectric metasurface (EDM) including dual-layer graphene (DLG). An EDM is a dielectric grating overlapped by two cladding layers, and it excites a Fano resonance. DLG is positioned inside the upper cladding layer to maximize light-graphene interaction. Thus, with a small change of the chemical potential (μ_c) of graphene, a resonance wavelength is tuned to switch the OFS on and off. First, a red-parity asymmetric Fano resonance is realized, and a sharp asymmetric lineshape is achieved by controlling the structural parameters of the EDM and the interaction between the Fano resonance and additional weak Fabry–Perot interference for efficient switching. The distance of a peak-to-dip wavelength ($\Delta\lambda_{p-d}$) and the change of chemical potential ($\Delta\mu_c$) for switching is analyzed by varying the duty cycle (DC) and grating thickness (t_g) of the EDM. Furthermore, switching contrast as a figure of merit (FoM) is analyzed. With DC of 0.5 and t_g of 70 nm, the OFS requires $\Delta\lambda_{p-d}$ of 7.3 nm and $\Delta\mu_c$ of 0.25 eV. The FoM of 0.97 is achieved. By adjusting the two parameters, the switching condition is tuned. In the case of a blue parity, the effect of the two parameters exhibits a similar trend to that of the red parity. The FoM, however, is lower due to the reversed parity.

1. Introduction

Ever since the unique spectral lineshape observed in quantum mechanical systems was explained by Ugo Fano [1], the renowned Fano resonance due to the interference between a discrete state and a continuum state has been widely used to understand the resonances found in guided-mode resonance (GMR) gratings, photonic crystals, plasmonic structures, and optical metasurfaces [2–6]. The Fano resonance, also known as GMR in one-dimensional (1D) dielectric gratings, has been used in the design of optical filters, broadband reflectors, and optical switches by tailoring design parameters such as grating thickness (t_g), period (Λ), and duty cycle (DC), defined as the ratio between the width of a high-refractive-index grating and Λ [2,3,7–14]. Ideally, a flat spectral response within the desired wavelength range is required for optical filters and broadband reflectors [2,8,9]. For optical sensing applications, a sharp symmetric Fano resonance lineshape is chosen [15–20], but a sharp asymmetric Fano resonance lineshape is preferable for optical switching [21]. Due to its unique asymmetric lineshape, switching contrast can be enhanced with a smaller shift of a resonance wavelength compared to the symmetric Fano resonance lineshape, also known as the Lorentzian lineshape [21–23]. Therefore, it is essential to manipulate a Fano resonance and achieve sharp asymmetric lineshape in a GMR structure for efficient switching.

For real-time switching of a resonance structure, a resonance wavelength should be actively tuned by changing the refractive index of a layer or a part of the structure. Diverse electro-optic materials such as liquid crystals, transparent conducting oxides, semiconductors, and so forth, have been employed to change the refractive index [5,22,24]. Recently, graphene has been used for optics and photonics applications due to its unique gapless property and the tunability of its refractive index [14,25–28]. Due to its gapless property, optical switching at a fixed resonance

#461706 https://doi.org/10.1364/OE.461706
Journal © 2022 Received 20 Apr 2022; revised 19 May 2022; accepted 20 May 2022; published 3 Jun 2022

wavelength has been achieved through the absorption of incident light and the reduction of reflected light by shifting the chemical potential (μ_c) of the graphene above and below half of the incident photon energy [13,14]. Like other optical switching structures using the enumerated electro-optic materials, optical switching using graphene is made possible by the shifting of the resonance wavelength via the electro-static gating of graphene [25]. However, to achieve switching, the chemical potential of graphene should be sufficiently tuned above half of the incident photon energy to avoid absorption in the graphene while keeping the intensity of the reflected or transmitted light as high as possible. Furthermore, for efficient switching, the interaction between the excited mode of a resonance structure and graphene should be large enough to change the resonance wavelength with a small change of μ_c.

Here, we propose an optical Fano switch (OFS) using an embedded dielectric metasurface (EDM) containing dual-layer graphene (DLG). An EDM, which is a 1D dielectric grating sandwiched between two cladding layers, excites a Fano resonance. DLG is put inside the upper cladding layer to enhance the light-graphene interaction. Then, a resonance wavelength is shifted by tuning μ_c of graphene to switch the OFS on and off. The asymmetry of a Fano resonance lineshape is sharpened by adjusting DC and t_g and additionally by tuning Fabry–Perot (FP) interference. As a result, an asymmetric lineshape with high switching contrast is achieved. Switching condition is then analyzed by varying two structural parameters: DC and t_g. The OFS is evaluated in terms of the distance between a peak wavelength and a dip wavelength ($\Delta\lambda_{p-d}$), the required change of chemical potential ($\Delta\mu_c$), and a figure of merit (FoM) defined to quantify switching contrast. The OFS with DC of 0.5 and t_g of 70 nm needs $\Delta\lambda_{p-d}$ of 7.3 nm and $\Delta\mu_c$ of 0.25 eV, and the FoM of 0.97 is achieved. By controlling the two parameters, the switching condition is selected. Similarly, with a blue parity, the effect of the two parameters exhibits a similar trend to that of the red parity. The FoM, however, is lower due to the reversed parity.

2. Methods: concept and consideration

A schematic illustration and its cross-section of an active two-port OFS structure are shown in Fig. 1(a) and 1(b). The OFS structure consists of an EDM, DLG as an electro-optic material [24,29–31], and a SiO_2/Si substrate. The EDM is a 1D dielectric metasurface surrounded by two dielectric cladding layers [13,14]. The metasurface is a 1D grating structure consisting of alternating high-refractive-index and low-refractive-index 1D grating bars. The high-index material is TiO_2 and the low-index material is SiO_2. The TiO_2 cladding layers are added to spread the resonance field distribution outside the metasurface and to increase the light-graphene interaction [13,14]. The DLG, which is two separate graphene layers, is employed to enhance the light-graphene interaction furthermore, and it can minimize the required change of chemical potential. The DLG is separated by a 10 nm thick HfO_2 layer, and each graphene layer can be electro-statically gated independently. The top graphene layer is covered by another 5 nm thick HfO_2 layer. The HfO_2 layers are added because they have a high dielectric constant and provide low doping of graphene [32,33]. The conductivity of graphene (σ_G) can be modeled using the Kubo model [31,34–36]. The in-plane complex permittivity of graphene was obtained from the conductivity as follows:

$$\varepsilon = 1 + \frac{i\sigma_G}{\omega\varepsilon_0 t_G}, \tag{1}$$

where ω is the angular frequency, ε_0 is the vacuum permittivity, and t_G is the thickness of the graphene. A t_G of 0.34 nm was used in the numerical simulation [31]. Switching can be conducted by tuning the μ_c of graphene with respect to the energy of incident light, $\hbar\omega$. For reflective-type switching, the graphene is electro-statically gated to reach the electro-refractive region where μ_c is above $\hbar\omega/2$ [29,30]. In the electro-refractive region, a change of μ_c alters the refractive index of graphene, and hence a resonance wavelength is shifted. The resonance mechanism of the OFS structure is illustrated in Fig. 1(c). Incident light (i) interacts with the

OFS structure which consequently reflects and transmits the incident light with a total reflection coefficient of r and transmission coefficient of t, respectively. In the EDM structure, GMR can be excited at a resonance angular frequency of ω_0, and some of the incident light is absorbed with an absorption probability of η_{abs} in the DLG [37]. Furthermore, the GMR is affected by the weak FP interference excited by the EDM and bottom Si substrate separated by the buried oxide (BOX) layer. At ω_0, the incident light resonantly interacts with the OFS structure, before leaking out with each decay probability of η_{dec} to the incident and exit regions. The total coefficient of each region is the sum of direct (r_d, t_d) and indirect parts (r_{id}, t_{id}). The direct parts are due to non-resonant effect, which can be described by replacing the metasurface with an effective medium layer. The indirect parts are caused by the resonant scattering of the OFS structure [5,38]. The representative reflectance spectra of the ON-state and OFF-state are shown in Fig. 1(d) depending on the μ_c of graphene. At μ_{c1} for the OFF-state, the dip reflectance is lowest at the center of the relative wavelength. When the chemical potential increases to μ_{c2} for the ON-state, the resonance wavelength is blue-shifted, the peak reflectance coinciding with the dip reflectance of the OFF-state. Consequently, by tuning μ_c above $\hbar\omega_0/2$, a Fano switch can be shifted from the ON-state to the OFF-state. For efficient switching in terms of a required wavelength shift ($\Delta\lambda_{p-d}$), an asymmetric lineshape rather than a symmetrical one is preferred [21,23]. Moreover, considering switching contrast [21,37], a parity factor (p) of +1 (red parity) of the asymmetric lineshape adopted here is preferred over a p of −1 (blue parity).

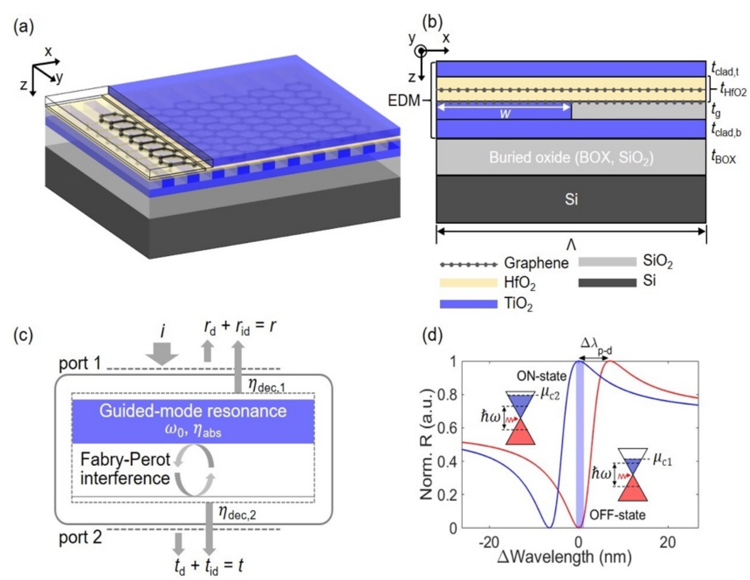

Fig. 1. Schematic of (a) a two-port OFS and (b) the cross-section of a unit cell with design parameters: period (Λ), width of a high-refractive-index grating bar (w), and thicknesses of each layer. (c) Schematic illustration of the resonance mechanism of the OFS structure excited primarily using guided-mode resonance interacting with additional FP interference. Incident light (i). Reflected and transmitted light from direct (r_d, t_d), and indirect process (r_{id}, t_{id}). (d) Representative reflectance spectrum of the ON-state and OFF-state based on a change of the μ_c of graphene and the corresponding shift of a peak-to-dip wavelength, $\Delta\lambda_{p-d}$.

Optics EXPRESS

3. Results and discussion

To investigate the switching condition of an OFS structure, a rigorous coupled-wave analysis (RCWA) method was employed and an in-house RCWA code was used for the numerical calculation of reflectance (R), transmittance (T), and absorptance (A) [10,13,14,39]. The design parameters of a representative OFS structure with a red parity (OFS-R) are summarized in Table 1. The OFS structure was designed for transverse-electric (TE) polarized light, the electric field component being parallel to the grating. Unless otherwise mentioned, the TE-polarized light was incident on the OFS with normal incidence. All the dielectric materials used here except graphene were assumed to be constants: $n_{TiO_2} = 2.411$, $n_{SiO_2} = 1.4381$, $n_{HfO_2} = 1.8766$, and $n_{Si} = 3.47$. In the case of graphene, the Kubo model was employed by assuming an intra-band relaxation time (τ) of 100 fs at room temperature, and Eq. (1) was used to obtain the dispersion of the complex permittivity of graphene. A theoretical analysis was conducted using Fano formulas to compare with the RCWA results and to understand the resonance property of the OFS structure. The numerical results of the reflectance and transmittance spectrum of the representative OFS-R structure without DLG in a wavelength range from 1970 nm to 2030 nm are shown in Fig. 2(a), denoted by a solid line. The reflectance and transmittance spectrum show an asymmetric Fano lineshape. At a short wavelength of 2002.0 nm, the reflectance drops to a minimum of 0.89%, and at a long wavelength of 2008.4 nm, the reflectance reaches a maximum of 99.39%. The distance between the peak and dip ($\Delta\lambda_{p-d}$) is 6.4 nm, and is related to the resonance sharpness, $\tilde{Q} = \lambda/\Delta\lambda_{p-d}$, where λ is the median of the two wavelengths [24]. Consequently, as $\Delta\lambda_{p-d}$ becomes smaller, the sharpness (or $\tilde{Q}$ factor) increases. The lossless two-port OFS-R structure was analyzed using the theoretical Fano formula, as follows:

$$\mathrm{T}(\delta) = |t_d|^2 + \frac{4\eta_1\eta_2}{1+\delta^2} + \frac{4|t_d|\sqrt{\eta_1\eta_2}(\delta\sin\Delta + \cos\Delta)}{1+\delta^2}, \tag{2}$$

where t_d is the amplitude of a direct transmission coefficient, $\delta = (\omega\text{-}\omega_0)/\gamma_{tot}$ is the normalized frequency, γ_{tot} (= $\gamma_1 + \gamma_2$) is the total decay rate into the two ports, $\eta_{1,2}$ (= $\gamma_{1,2}/\gamma_{tot}$) is the decay probability into each port, $\Delta = p\cdot\cos^{-1}(-|t_d|/\beta^{1/2})$ is the phase difference between the direct and indirect transmission at the resonance wavelength [37], and $\beta = 4\eta_1\eta_2/(\eta_1+\eta_2)^2$ is the coupling-symmetry factor. First, the t_d of the lossless OFS-R can be calculated by replacing the grating with a homogeneous layer with an effective refractive index, $n_{g,eff}$. The 0^{th}-order effective medium theory ($n^2_{g,eff} = DC\cdot n^2_{TiO_2} + (1-DC)\cdot n^2_{SiO_2}$) was used to obtain the effective refractive index for TE polarization [5,7,40]. Since the wavelength of the minimum transmittance is longer than that of the maximum transmittance, the p is +1 [21,37].

Table 1. Design parameters for the representative OFS-R

Λ (nm)	DC	t_g (nm)	$t_{clad,t}$(nm)	$t_{clad,b}$ (nm)	t_{BOX} (nm)
1220	0.5	70	70	90	1750

Consequently, with the estimated t_d and a p of +1, a theoretical fit to the RCWA results was conducted. The theoretical spectra are superimposed on the solid line using a square-dotted line. The theoretical result is well fitted with the numerical one. From the results, γ_{tot}, ω_0, and $\eta_{1,2}$ are obtained. γ_{tot} is ~1.445 THz, and η_1 and η_2 are estimated to be ~0.545 and ~0.455, respectively. Furthermore, the q-parameter defined as -tanΔ is ~1.203. Because the q-parameter deviates from 1, the resonance wavelength (λ_0) of 2004.5 nm differs from 2005.2 nm, which is the median of the peak and dip wavelengths [6]. The calculated quality factor of $Q = \omega_0/2\gamma_{tot}$ is ~324, similar to $\tilde{Q}$ ~313. The excited mode profile of $|E_y|$ at the λ_0 is shown in Fig. 2(d). The mode profile shows the fundamental mode with a maximum $|E_y|$ of 17.42. The field intensity is strong in the metasurface and cladding layers and gradually decreases away from the EDM. For active switching, the OFS-R structure includes DLG near the metasurface to enhance the light-graphene

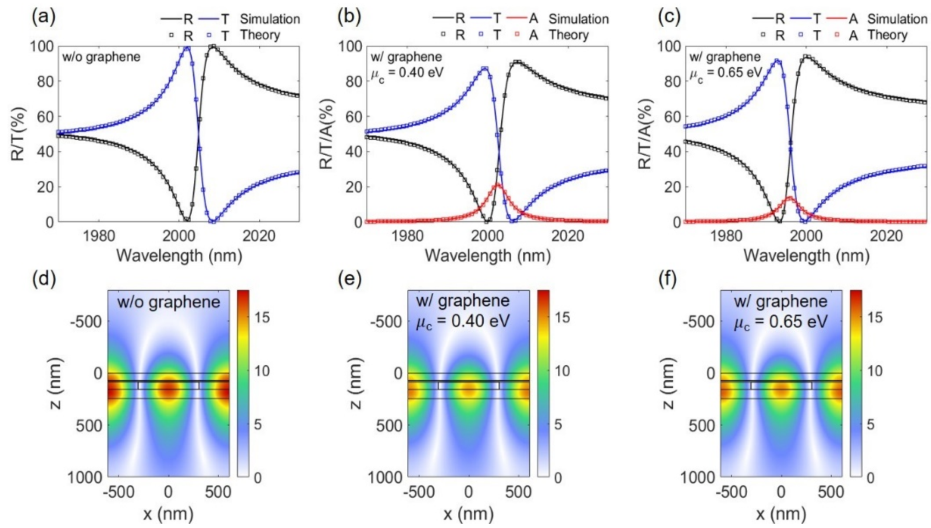

Fig. 2. (a) Reflectance and transmittance spectrum of a representative OFS-R without DLG and (d) its field profile at the corresponding resonance wavelength. Reflectance, transmittance, and absorbance spectrum of the OFS structure with DLG and its field profile at each resonance wavelength: μ_c of (b), (e) 0.40 eV and (c), (f) 0.65 eV.

interaction and increase the shift of the resonance wavelength. Since the OFS-R structure is now a lossy two-port system, it was analyzed using the modified Fano formula, as follows:

$$\mathrm{T_{lossy}}(\delta) = \eta_{\mathrm{dec}}|t_{\mathrm{d}}|^2\frac{(q+\delta)^2}{1+\delta^2} - \beta\frac{\eta_{\mathrm{dec}}\eta_{\mathrm{abs}}}{1+\delta^2} + \eta_{\mathrm{abs}}|t_{\mathrm{d}}|^2, \tag{3}$$

where $\eta_{\mathrm{dec}} = \eta_1 + \eta_2 = 1 - \eta_{\mathrm{abs}}$ is the sum of the two decay probabilities and η_{abs} ($\gamma_{\mathrm{abs}}/\gamma_{\mathrm{tot}}$) is the absorption probability of DLG [37]. Then, the reflectance was calculated, as follows:

$$\mathrm{R_{lossy}}(\delta) = 1 - \mathrm{T_{lossy}}(\delta) - \frac{4\eta_1\eta_{\mathrm{abs}}}{1+\delta^2}, \tag{4}$$

where the third term on the right-hand side expresses the resonant absorption [37]. Figure 2(b) shows the reflectance, transmittance, and absorptance spectrum of the OFS-R with DLG at μ_c of 0.4 eV. Since the OFS-R includes DLG, the incident light is absorbed. The maximum absorptance (A_{max}) is 21.04% at λ_0 of 2002.5 nm. The peak and dip reflectance (R_{peak} and R_{dip}) are 90.85% and 0.03% at 2007.3 nm and 2000.0 nm, respectively, and $\Delta\lambda_{p-d}$ is 7.3 nm. The theoretical result based on Eq. (3) is overlaid on the numerical results with a square-dotted line. The total decay rate of γ_{tot} is 1.610 THz, and the three probabilities of η_1, η_2, and η_{abs} are ~0.476, ~0.413, and ~0.111, respectively. It is noteworthy that the ratio of (η_1+η_2) to η_{abs} is far from 1, the critical coupling condition [13,14]. The absorptance is small, and therefore the OFS is suitable for reflective-type switching. The q-parameter is ~1.199 and the Q factor is 291. Since the $\Delta\lambda_{p-d}$ increases due to the absorption in graphene, the Q factor decreases. Moreover, the increased γ_{tot} is additional evidence of the decreasing Q factor. The excited mode profile $|E_y|$ at the λ_0 of 2002.5 nm is shown in Fig. 2(e). Since DLG absorbs some of the incident light, the maximum $|E_y|$ is reduced to 15.38. However, the mode profile is still conserved. The resultant spectrum changes when μ_c increases to 0.65 eV as shown in Fig. 2(c). The R_{peak} and R_{dip} are 93.62% and 0.04% at 2000.1 nm and 1993.2 nm, respectively, and $\Delta\lambda_{p-d}$ is 6.9 nm. The overall R/T/A spectra at μ_c of 0.65 eV are blue-shifted compared to those at μ_c of 0.40 eV. The

Optics EXPRESS

peak reflectance increases because μ_c moves further into the electro-refractive region [29,30]. Consequently, the absorptance of the OFS-R reduces to 13.78% at λ_0 of 1995.8 nm. The decay rate of γ_{tot} is 1.545 THz, and the three decay probabilities of η_1, η_2, and η_{abs} are ~0.511, ~0.422, and ~0.067, respectively. The q-parameter and Q factor are 1.195 and 304, respectively. Since the γ_{tot} decreases again, the Q factor increases accordingly. The excited mode profile at the λ_0 of 1995.8 nm is shown in Fig. 2(f), and the maximum $|E_y|$ is 15.89. Since the absorbance slightly decreases compared to the case when the μ_c is 0.4 eV, the maximum $|E_y|$ increases.

To reveal the effect of a BOX layer on the Fano resonance lineshape, the reflectance maps as a function of the BOX thickness and wavelength were calculated, then the Fano resonance lineshape was analyzed at two different BOX thicknesses as shown in Fig. 3. In the OFS structure, there is weak FP interference as well as the GMR. To eliminate the GMR effect, the metasurface of the EDM structure in the representative OFS-R is replaced with an effective homogeneous layer, and the reflectance is then calculated without graphene as shown in Fig. 3(a) [7,40]. There is weak FP interference caused by the bottom Si and the top homogeneous layers separated by the BOX layer. The dip and peak regularly occur as the BOX thickness increases. The collective effects of the FP interference and GMR in the OFS-R at μ_c of 0.65 eV (ON-state) and 0.40 eV (OFF-state) are shown in Fig. 3(b) and 3(c), respectively. Overall, the FP dip and peak lines are distorted and broken around the GMR. Near the left-hand side before the GMR, the reflectance is lower than that at the right-hand side. In particular, below a BOX thickness of 1000 nm, the peak reflectance starts to decrease, and below 500 nm, there is no GMR. This can be attributed to the evanescent field in the EDM starting to interact with the bottom Si layer. As a result, the GMR disappears [12]. When the μ_c of graphene decreases to 0.40 eV, the GMR region is red-shifted as shown in Fig. 3(c). In addition, the reflectance peaks slightly decrease due to the incremental absorbance in DLG around the GMR. However, the overall shape of the reflectance map is consistent. To compare the Fano resonance lineshape, the reflectance spectrum of the OFS-R with a BOX thickness of 1375 nm and 1750 nm for each state is shown in Fig. 3(d). To evaluate the switching condition, a FoM is defined to be $(R_{peak}-R_{dip})/(R_{peak}+R_{dip})$ [22]. Furthermore, the required change of μ_c ($\Delta\mu_c$) is considered for switching. The reflectance spectrum of the upper panel at a BOX thickness of 1375 nm shows the symmetric lineshape at two different μ_c values. At μ_c of 0.65 eV, R_{peak} is 89.86% at 1999.3 nm. As the μ_c decreases to 0.40 eV, R_{peak} is 86.62% at 2006.1 nm and R is 37.84% at 1993.3 nm. With $\Delta\mu_c$ of 0.25 eV, the resonance wavelength is red-shifted by 6.8 nm. To compare the switching condition by considering a finite full width at half maximum (FWHM) of the incident beam, the average reflectance is calculated within a 2 nm window (highlighted by a light blue box). Unless otherwise mentioned, the width of the window is fixed at 2 nm. The average reflectance (R_{avg}) at 1999.3 nm is 89.22% and 37.67% for each state, respectively. The difference in the average reflectance (ΔR_{avg}) of the ON-state and OFF-state is 51.55% and the FoM is ~0.40 with $\Delta\mu_c$ of 0.25 eV. The reflectance spectra of the lower panel show the asymmetric Fano lineshape at the two states. The resonance wavelength is blue-shifted as μ_c increases. At μ_c of 0.65 eV, R_{peak} is 93.62% at 2000.1 nm. At a lower μ_c of 0.40 eV, the R_{peak} and R_{dip} are 90.85% at 2007.3 nm and 0.03% at 2000.0 nm, respectively, and $\Delta\lambda_{p-d}$ is 7.3 nm. The difference in the average peak ($R_{avg,peak}$) and dip reflectance ($R_{avg,dip}$) is 92%, and the FoM is 0.97. The asymmetric Fano lineshape improves the reflectance difference between the ON-state and OFF-state with the same $\Delta\mu_c$ compared to the symmetric lineshape. As a result, the asymmetric Fano lineshape exhibits better switching performance than the symmetric one. It is noticeable that at a BOX thickness of 1750 nm where the peak of the FP interference is positioned, the asymmetric Fano resonance can be obtained. Conversely, the symmetric line shape is achieved near the dip position of the FP interference [41]. Consequently, the BOX thickness should be chosen near the peak position of the background FP interference.

The effect of the DC on the reflectance was calculated as shown in Fig. 4. Figure 4(a) shows the reflectance map of the OFS-R without DLG as a function of the DC and wavelength. It

Optics EXPRESS

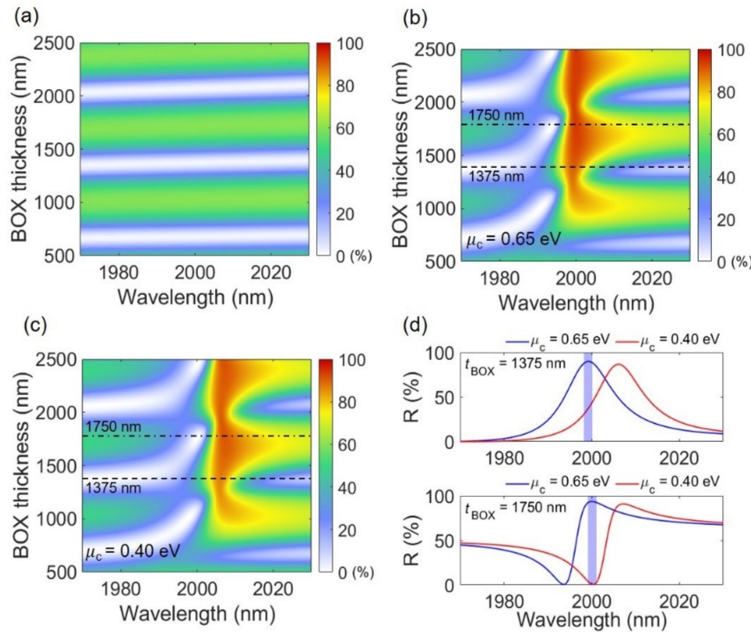

Fig. 3. (a) Reflectance map of the representative OFS-R in which the metasurface is replaced with an effective medium without DLG and (b), (c) of the representative OFS with μ_c of 0.65 eV (ON-state) and 0.40 eV (OFF-state) as a function of the BOX thickness and wavelength. (d) Reflectance spectra of the OFS-R with a BOX thickness of 1375 nm (upper panel) and 1750 nm (lower panel) at the ON-state and OFF-state. The ON-state and OFF-state for two representative Fano resonance lineshapes demonstrate the switching contrast in the light blue box.

shows an elongated *S*-like shape with two sharp ends. Near the middle of the DC region between 0.4 and 0.6, the shift of the resonance wavelength is small compared to both ends of the DC region. In addition, the resonance linewidth is broad in the middle region, but both ends possess sharp linewidths. The reflectance map of the OFS-R shows a red-parity without regard to the DC. Consequently, in the shorter wavelength region below the resonance wavelength, it exhibits low reflectance. As the wavelength approaches the resonance wavelength from the shorter wavelength, the reflectance drops to ~0%. Subsequently, the reflectance abruptly increases around the resonance wavelength and reaches a maximum, before slightly decreasing again. The abrupt change of the reflectance from the dip to the peak grows steeper as the DC increases beyond 0.6 or as the DC decreases below 0.4. With DLG at μ_c of 0.65 eV, the overall reflectance map exhibits a similar shape except for the overall shift of the *S*-like resonance region toward the shorter wavelengths as shown in Fig. 4(b). Even though μ_c further decreases to 0.40 eV, the overall reflectance map still preserves the *S*-like shape, except that the peak reflectance is further reduced due to the enhanced absorption in graphene. However, the parity of the asymmetric Fano lineshape is maintained when μ_c is tuned for switching. To compare the switching condition at three different DCs of 0.3, 0.5, and 0.7, the reflectance spectra at the ON-state and OFF-state are shown in Fig. 4(d)–4(f). With DC of 0.3, the R_{peak} and R_{dip} of the OFF-state are 87.57% at 2000.6 nm and 0.05% at 1995.1 nm, respectively, and $\Delta\lambda_{p-d}$ is 5.5 nm. R_{peak} of the ON-state is 91.29% at 1993.5 nm as indicated by the blue-dotted line in Fig. 4(d). Since the peak of the ON-state spectrum moves lower than the dip of the OFF-state, the μ_c for the ON-state is lowered to 0.575 eV. As a result, the adjusted ON-state peak, denoted by a blue-solid line, is aligned with the OFF-state dip at 1995.1 nm with a reflectance of 92.02%. Consequently, with DC of

0.3, it requires $\Delta\mu_c$ of 0.175 eV for switching. The $R_{avg,peak}$ and $R_{avg,dip}$ are 91.22% and 1.82%, respectively, and ΔR_{avg} is 89.4%. Thus, the FoM is 0.96 with $\Delta\mu_c$ of 0.175 eV. For the purpose of comparison, the results of the representative OFS-R spectra with DC of 0.5 are shown in Fig. 4(e). A larger $\Delta\mu_c$ of 0.25 eV is required since $\Delta\lambda_{p-d}$ at μ_c of 0.4 eV is 7.3 nm. However, it exhibits an improved ΔR_{avg} of 92% and FoM of 0.97. Figure 4(f) shows the reflectance spectra of the OFS with DC of 0.7. The R_{peak} and R_{dip} of the OFF-state are 87.30% at 2016.8 nm and 0.0% at 2011.8 nm, respectively. $\Delta\lambda_{p-d}$ at OFF-state is 5.0 nm. The peak reflectance of the ON-state at μ_c of 0.65 eV is 90.55% at 2009.5 nm. To align the ON-state with the OFF-state, μ_c is reduced to 0.545 eV. Then, the peak reflectance is 91.62% at 2011.8 nm, and the required $\Delta\mu_c$ is 0.145 eV. The $R_{avg,peak}$ and $R_{avg,dip}$ are 89.99% and 2.73%, respectively, and ΔR_{avg} is 86.76%. The FoM is 0.94. Therefore, the switching can be conducted with a lower $\Delta\mu_c$ by adjusting the DC, but at the expense of the FoM.

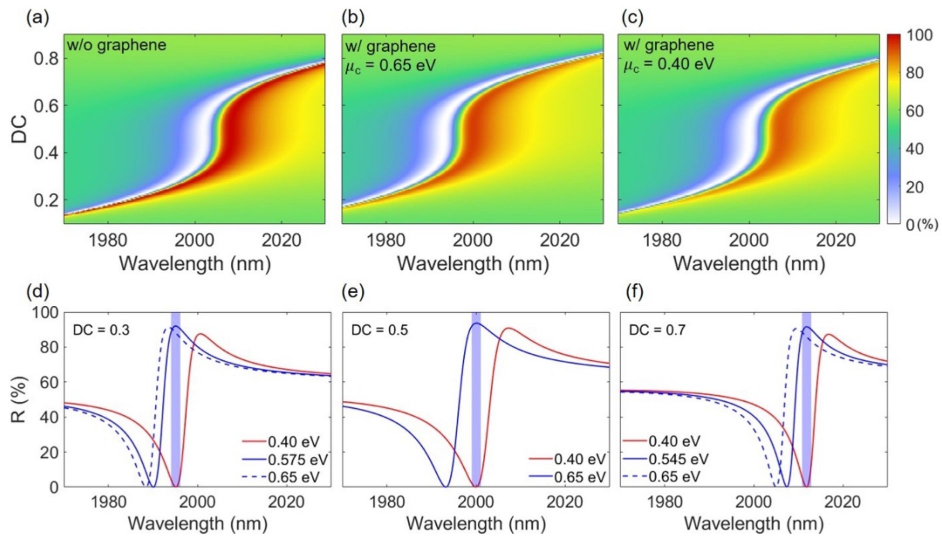

Fig. 4. Reflectance map as a function of the DC and wavelength (a) without graphene and (b), (c) with graphene at μ_c of 0.65 eV (ON-state) and 0.40 eV (OFF-state). (d-f) The reflectance spectra with three different DCs of 0.3, 0.5, and 0.7 present the ON-state and OFF-state. The required μ_c of the ON-state varies depending on the DC.

The effect of the grating thickness of an OFS-R on an asymmetric Fano resonance lineshape was investigated by calculating the optical reflectance map at the ON-state and OFF-state. The reflectance map as a function of grating thickness and wavelength is shown in Fig. 5(a) and 5(b). The other parameters are the same as those summarized in Table 1. The width of an asymmetric Fano lineshape around the resonance wavelength widens as the grating thickens for both μ_c of 0.65 eV as the ON-state and 0.40 eV as the OFF-state. As μ_c decreases from 0.65 eV to 0.40 eV, as shown in Fig. 5(a) and 5(b), the resonance region shifts downward. With a lower μ_c, the peak reflectance decreases because the graphene is close to the electro-absorption region and the absorption increases. Nevertheless, the overall shape of the reflectance map and the parity remain the same. Figure 5(c)–5(e) shows the ON-state and OFF-state spectra with a grating thickness of 50 nm, 70 nm, and 90 nm. For the purpose of comparison, the representative OFS-R spectra with a grating thickness of 70 nm is also shown. With a grating thickness of 50 nm, the R_{peak} and R_{dip} of the OFF-state are 85.62% at 1990.8 nm and 0.37% at 1986.0 nm, respectively, and $\Delta\lambda_{p-d}$ is 4.8 nm. R_{peak} of the ON-state is 89.83% at 1983.1 nm. Since the peak position of the ON-state moves further away from the dip position of the OFF-state, the μ_c for the ON-state decreases to

0.53 eV. As a result, R_{peak} of 91.09% is achieved at 1985.9 nm, and the peak and dip positions are aligned. Moreover, the $R_{avg,peak}$ and $R_{avg,dip}$ are 89.99% and 3.23%, respectively. Therefore, ΔR_{avg} is 86.76% and the FoM is 0.93. The required $\Delta\mu_c$ for switching is 0.13 eV, which is 0.12 eV smaller than that of the representative OFS-R. In addition, the spectrum around the dip and peak is narrow and sharp. Consequently, when incident light possesses a narrow FWHM, an OFS-R with a thin grating can be selected to filter unwanted light. With a grating thickness of 90 nm, the R_{peak} and R_{dip} of the OFF-state are 96.66% at 2022.6 nm and 0.26% at 2012.1 nm, respectively, and $\Delta\lambda_{p-d}$ is 10.5 nm. With μ_c of 0.65 eV, the R_{peak} of the ON-state is 95.51% at 2015.7 nm. Since the ON-state peak is not well aligned with the OFF-state dip, μ_c increases further. With μ_c of 0.85 eV, R_{peak} of 94.44% is achieved at 2012.0 nm and is aligned with R_{dip}. The average peak and dip reflectances are 94.25% and 0.71%, respectively. By applying $\Delta\mu_c$ of 0.45 eV, ΔR_{avg} of 93.54% and FoM of 0.98 are achieved. The thicker grating possesses the highest FoM, but requires the largest $\Delta\mu_c$. Within the light blue box region, there is an almost flat spectrum around the peak and dip. Similar to the effect of the DC on switching, the $\Delta\lambda_{p-d}$ or a slope of the spectral dispersion around a resonance wavelength can be controlled by tailoring the grating thickness. Not only that the possibility of controlling the asymmetric lineshape, but the resonance wavelength can also be tuned further into the longer mid-infrared wavelength range by controlling the structural parameters of the EDM [13].

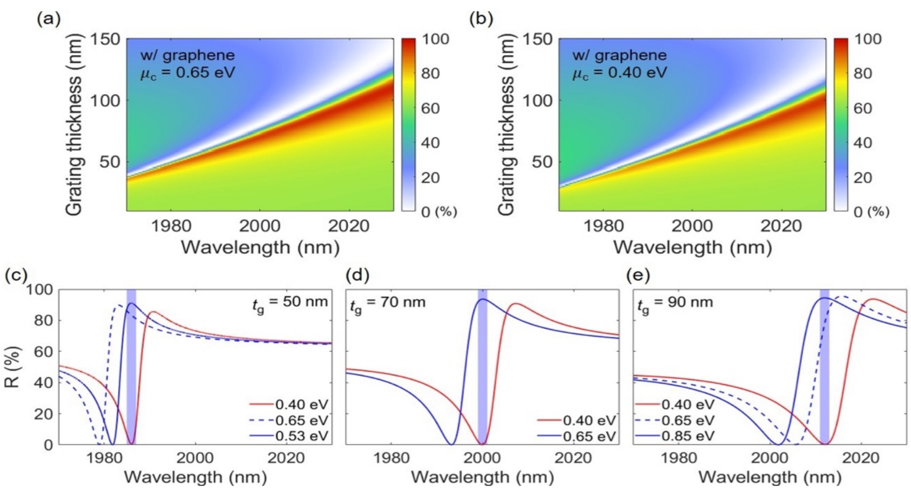

Fig. 5. (a), (b) Reflectance map as a function of grating thickness, t_g and wavelength at μ_c of 0.65 eV (ON-state) and 0.40 eV (OFF-state). (c)-(e) The ON-state and OFF-state reflectance spectra at three different t_g of 50, 70, and 90 nm. The required μ_c for the ON-state increases as t_g thickens.

To compare the effect of the parity of an asymmetric lineshape on the switching condition, the opposite blue-parity is investigated. For the blue-parity, the spectrum is flipped along the resonance wavelength compared to the red-parity. Figure 6(a) shows the ON-state and OFF-state spectra of the representative OFS with a blue-parity (OFS-B), and the design parameters of which are shown in Table 2.

Table 2. Design parameters for the representative OFS-B

Λ (nm)	DC	t_g (nm)	$t_{clad,t}$ (nm)	$t_{clad,b}$ (nm)	t_{BOX} (nm)
1000	0.3	100	200	220	1720

Optics EXPRESS

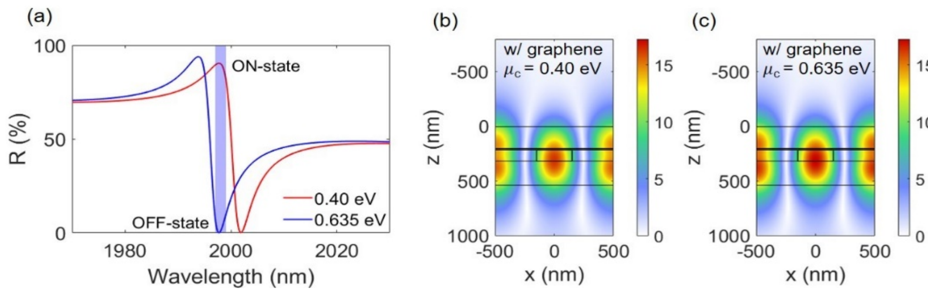

Fig. 6. (a) The representative ON-state and OFF-state reflectance spectrum of an OFS-B structure with a blue-parity. The ON-state is with a low μ_c of 0.4 eV and a high μ_c of 0.635 eV. (b), (c) The field profile at the corresponding resonance wavelength for each state.

Even though it possesses the opposite parity, as μ_c increases, the spectrum is blue-shifted much like the case of the red-parity. Therefore, a peak reflectance with a lower μ_c of 0.40 eV is now the ON-state, as shown in Fig. 6(a). The R_{peak} and R_{dip} of the ON-state are 90.37% at 1997.7 nm and 0.13% at 2001.9 nm, respectively, and $\Delta\lambda_{p-d}$ is 4.2 nm. As μ_c increases, the resonance wavelength is blue-shifted. The dip position of the reflectance spectrum at μ_c of 0.635 eV for the OFF-state is aligned with the ON-state peak. The switching is achieved with $\Delta\mu_c$ of 0.135 eV. The $R_{avg,peak}$ and $R_{avg,dip}$ within the light blue box are 89.53% and 4.34%, respectively. As a result, the ΔR_{avg} is 85.19% and FoM is 0.90. Figure 6(b) and 6(c) show the mode profile, $|E_y|$, of the ON-state at λ_0 of 2000.5 nm and the OFF-state at λ_0 of 1996.3 nm. The field profile shows the fundamental mode, but with an elongated mode shape along the *z*-direction compared to that of the OFS-R. This is because the EDM is sandwiched by thicker top and bottom cladding layers. To enhance the FoM of the OFS, the reflectance difference between the ON-state and OFF-state should be larger. However, the ON-state of the OFS-B is set with a lower μ_c. As a result, the μ_c of graphene is close to the electro-absorption region and the peak reflectance decreases further. As a result, the FoM of the OFS-B is lower than that of the OFS-R, making the red-parity more suitable than the blue-parity.

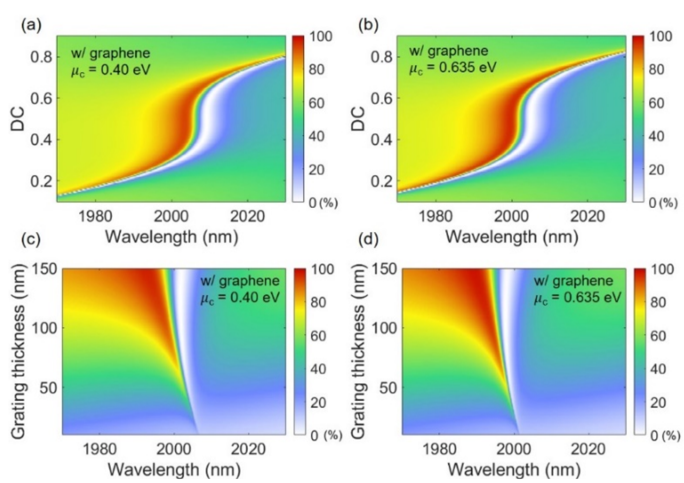

Fig. 7. (a,b) Reflectance map of the representative OFS-B as a function of the DC and wavelength at μ_c of 0.40 eV (ON-state) and 0.635 eV (OFF-state). (c), (d) Reflectance map as a function of t_g and wavelength at μ_c of 0.40 eV (ON-state) and 0.635 eV (OFF-state).

Optics EXPRESS

To further understand the representative OFS-B, the effect of the DC and grating thickness on switching conditions is investigated by calculating the reflectance map as shown in Fig. 7. Figure 7(a) and 7(b) show the reflectance map as a function of the DC and wavelength at μ_c of 0.4 eV and 0.635 eV. The reflectance maps possess the trace of the resonance wavelength with an elongated *S*-shape, much like that of the OFS-R. However, the difference is that the shorter wavelength regions below the resonance wavelength show higher reflectance than that of the longer wavelength region because of the blue-parity. The reflectance maps as a function of grating thickness and wavelength are shown in Fig. 7(c) and 7(d) for each state. As μ_c increases to switch from the ON-state to the OFF-state, the resonance wavelength is blue-shifted. As the grating thickness increases for both states, the resonance wavelength shifts to a shorter wavelength. This is contrary to the representative OFS-R, which exhibits red-shifting. Nevertheless, the peak-to-dip wavelength distance widens as the grating thickness increases, as shown in the OFS-R.

4. Conclusions

We proposed and analyzed an OFS using an EDM containing DLG. The switching was realized by changing the μ_c of graphene and shifting the resonance wavelength of the OFS. For efficient switching, an asymmetric Fano resonance lineshape with a red-parity was excited by using the interaction between a Fano resonance and FP interference. Using an asymmetric lineshape with the red-parity, the effect of the two design parameters of DC and grating thickness on switching conditions was analyzed in terms of $\Delta\mu_c$ and FoM. When the DC increased beyond ~0.6 or decreased below ~0.4, $\Delta\lambda_{p-d}$ decreased. In the case of DC around 0.5, $\Delta\lambda_{p-d}$ was almost constant. As the grating became thick, $\Delta\lambda_{p-d}$ increased, and hence the required $\Delta\mu_c$ was increased. The FoM, however, could be lower as $\Delta\lambda_{p-d}$ decreased due to the increased absorption around the resonance wavelength. In the case of a blue-parity, the effect of the DC on the switching condition was similar to the OFS with the red-parity. However, the FoM was slightly lower because the ON-state suffered more absorption. Due to the gapless property of graphene, DLG as electro-optic material can be used even in a longer wavelength range. Therefore, the design principle and the property of the OFS can be used in longer mid-infrared applications.

Funding. Ministry of Science and ICT, South Korea (2019-0-00002).

Acknowledgments. This work was supported by the Institute of Information & Communications Technology Planning & Evaluation (IITP) grant funded by the Korea government (MSIT) (No. 2019-0-00002, Development of Optical Cloud Networking Core Technology)

Disclosures. The authors declare no conflicts of interest.

Data availability. The data that support the findings of this study are available from the corresponding author upon reasonable request.

References

1. A. E. Miroshnichenko, S. Flach, and Y. S. Kivshar, "Fano resonances in nanoscale structures," Rev. Mod. Phys. **82**(3), 2257–2298 (2010).
2. S. S. Wang and R. Magnusson, "Theory and applications of guided-mode resonance filters," Appl. Opt. **32**(14), 2606–2613 (1993).
3. A. Taghizadeh, G. C. Park, J. Mørk, and I.-S. Chung, "Hybrid grating reflector with high reflectivity and broad bandwidth," Opt. Express **22**(18), 21175–21184 (2014).
4. S.-E. Mun, H. Yun, C. Choi, S.-J. Kim, and B. Lee, "Enhancement and switching of Fano resonance in metamaterial," Adv. Opt. Mater. **6**(17), 1800545 (2018).
5. S.-J. Kim, I. Kim, S. Choi, H. Yoon, C. Kim, Y. Lee, C. Choi, J. Son, Y. W. Lee, J. Rho, and B. Lee, "Reconfigurable all-dielectric Fano metasurfaces for strong full-space intensity modulation of visible light," Nanoscale Horiz. **5**(7), 1088–1095 (2020).
6. T. T. Hoang, Q. M. Ngo, D. L. Vu, and H. P. T. Nguyen, "Controlling Fano resonances in multilayer dielectric gratings towards optical bistable devices," Sci. Rep. **8**(1), 16404 (2018).
7. W. Stork, N. Streibl, H. Haidner, and P. Kipfer, "Artificial distributed-index media fabricated by zero-order gratings," Opt. Lett. **16**(24), 1921–1923 (1991).
8. R. Magnusson and S. S. Wang, "Transmission bandpass guided-mode resonance filters," Appl. Opt. **34**(35), 8106–8109 (1995).

9. G. C. Park, A. Taghizadeh, and I.-S. Chung, "Hybrid grating reflectors: origin of ultrabroad stopband," Appl. Phys. Lett. **108**(14), 141108 (2016).
10. G. C. Park and K. Park, "Critically coupled Fabry-Perot cavity with high signal contrast for refractive index sensing," Sci. Rep. **11**(1), 19575 (2021).
11. G. C. Park, W. Xue, A. Taghizadeh, E. Semenova, K. Yvind, J. Mørk, and I.-S. Chung, "Hybrid vertical-cavity laser with lateral emission into a silicon waveguide," Laser Photonics Rev. **9**(3), L11–L15 (2015).
12. G. C. Park, W. Xue, M. Piels, D. Zibar, J. Mørk, E. Semenova, and I.-S. Chung, "Ultrahigh-speed Si-integrated on-chip laser with tailored dynamic characteristics," Sci. Rep. **6**(1), 38801 (2016).
13. G. C. Park and K. Park, "Dual-guiding-layer resonance structure with an embedded metasurface for quasi-critical coupling without a perfect mirror," Sci. Rep. **10**(1), 16014 (2020).
14. G. C. Park and K. Park, "Tunable dual-wavelength absorption switch with graphene based on an asymmetric guided-mode resonance structure," Opt. Express **29**(5), 7307–7320 (2021).
15. J. Chen, C. Peng, S. Qi, Q. Zhang, C. Tang, X. Shen, H. Da, L. Wang, and G.-S. Park, "Photonic microcavity-enhanced magnetic plasmon resonance of metamaterials for sensing applications," IEEE Photonics Technol. Lett. **31**(2), 113–116 (2019).
16. J. Chen, H. Nie, C. Tang, Y. Cui, B. Yan, Z. Zhang, Y. Kong, Z. Xu, and P. Cai, "Highly sensitive refractive-index sensor based on strong magnetic resonance in metamaterials," Appl. Phys. Express **12**(5), 052015 (2019).
17. J. Chen, S. Qi, X. Hong, P. Gu, R. Wei, C. Tang, Y. Huang, and C. Zhao, "Highly sensitive 3D metamaterial sensor based on diffraction coupling of magnetic plasmon resonance," Results Phys. **15**(1), 102791 (2019).
18. J. Chen, S. Chen, P. Gu, Z. Yan, C. Tang, Z. Xu, B. Liu, and Z. Liu, "Electrically modulating and switching infrared absorption of monolayer graphene in metamaterials," Carbon **162**(1), 187–194 (2020).
19. J. Chen, Y. Kuang, P. Gu, S. Feng, Y. Zhu, C. Tang, Y. Guo, Z. Liu, and F. Gao, "Strong magnetic plasmon resonance in a simple metasurface for high-quality sensing," J. Lightwave Technol. **39**(13), 4525–4528 (2021).
20. J. Chen, C. Yang, P. Gu, Y. Kuang, C. Tang, S. Chen, and Z. Liu, "High sensing properties of magnetic plasmon resonance by strong coupling in three-dimensional metamaterials," J. Lightwave Technol. **39**(2), 562–565 (2021).
21. D. Bekele, Y. Yu, K. Yvind, and J. Mork, "In-plane photonic crystal devices using Fano resonances," Laser Photonics Rev. **13**(12), 1900054 (2019).
22. W. Zhao, H. Jiang, B. Liu, Y. Jiang, C. Tang, and J. Li, "Fano resonance based optical modulator reaching 85% modulation depth," Appl. Phys. Lett. **107**(17), 171109 (2015).
23. Y. Yu, W. Xue, H. Hu, L. K. Oxenløwe, K. Yvind, and J. Mork, "All-optical switching improvement using photonic-crystal Fano structures," IEEE Photonics J. **8**(2), 1–8 (2016).
24. E. Lee, I. C. Seo, S. C. Lim, H. Y. Jeong, and Y. C. Jun, "Active switching and tuning of sharp Fano resonances in the mid-infrared spectral region," Opt. Express **24**(22), 25684–25696 (2016).
25. H. S. Lee, J. Y. Kwak, T.-Y. Seong, G. W. Hwang, W. M. Kim, I. Kim, and K.-S. Lee, "Optimization of tunable guided-mode resonance filter based on refractive index modulation of graphene," Sci. Rep. **9**(1), 19951 (2019).
26. J. Wang, X. Wang, H. Shao, Z.-D. Hu, G. Zehng, and F. Zhang, "Peak modulation in multicavity-coupled graphene-based waveguide system," Nanoscale Res. Lett. **12**(1), 9 (2017).
27. Z. Bao, J. Wang, Z.-D. Hu, A. Balmakou, S. Khakhomov, Y. Tang, and C. Zhang, "Coordinated multi-band angle insensitive selection absorber based on graphene metamaterials," Opt. Express **27**(22), 31435–31445 (2019).
28. J. Hu, Y. Huang, Y. Chen, Z.-D. Hu, J. Wu, and J. Wang, "High-sensitivity multi-channel refractive-index sensor based on a graphene-based hybrid Tamm plasmonic structure," Opt. Mater. Express **11**(11), 3833–3843 (2021).
29. M. Liu, X. Yin, E. Ulin-Avila, B. Geng, T. Zentgraf, L. Ju, F. Wang, and X. Zhang, "A graphene-based broadband optical modulator," Nature **474**(7349), 64–67 (2011).
30. M. Mohsin, D. Neumaier, D. Schall, M. Otto, C. Matheisen, A. L. Giesecke, A. A. Sagade, and H. Kurz, "Experimental verification of electro-refractive phase modulation in graphene," Sci. Rep. **5**(1), 10967 (2015).
31. V. Sorianello, G. De Angelis, T. Cassese, M. Midrio, M. Romagnoli, M. Mohsin, M. Otto, D. Neumaier, I. Asselberghs, J. Van Campenhout, and C. Huyghebaert, "Complex effective index in graphene-silicon waveguides," Opt. Express **24**(26), 29984–29993 (2016).
32. X. Wang, Z. Cheng, K. Xu, H. K. Tsang, and J.-B. Xu, "High-responsivity graphene/silicon-heterostructure waveguide photodetectors," Nat. Photonics **7**(11), 888–891 (2013).
33. M. A. Giambra, A. Benfante, R. Pernice, V. Miseikis, F. Fabbri, C. Reitz, W. H. P. Pernice, R. Krupke, E. Calandra, S. Stivala, A. C. Busacca, and R. Danneau, "Graphene field-effect transistors employing different thin oxide films: a comparative study," ACS Omega **4**(1), 2256–2260 (2019).
34. Y.-L. Liao and Y. Zhao, "Graphene-based tunable ultra-narrowband mid-infrared TE-polarization absorber," Opt. Express **25**(25), 32080–32089 (2017).
35. P. Sun, C. You, A. Mahigir, T. Liu, F. Xia, W. Kong, G. Veronis, J. P. Dowling, L. Dong, and M. Yun, "Graphene-based dual-band independently tunable infrared absorber," Nanoscale **10**(33), 15564–15570 (2018).
36. Y.-L. Liao, H. Wang, Y. Zhao, X. Chen, J. Wu, and Z. Chen, "Small-angle ultra-narrowband tunable mid-infrared absorber composing from graphene and dielectric metamaterials," Coatings **11**(7), 825 (2021).
37. J. W. Yoon and R. Magnusson, "Fano resonance formula for lossy two-port systems," Opt. Express **21**(15), 17751–17759 (2013).
38. K. X. Wang, Z. Yu, S. Sandhu, and S. Fan, "Fundamental bounds on decay rates in asymmetric single-mode optical resonators," Opt. Lett. **38**(2), 100–102 (2013).

Optics EXPRESS

39. M. G. Moharam, E. B. Grann, D. A. Pommet, and T. K. Gaylord, "Formulation for stable and efficient implementation of the rigorous coupled-wave analysis of binary gratings," J. Opt. Soc. Am. A **12**(5), 1068–1076 (1995).
40. M. Foldyna, R. Ossikovski, A. D. Martino, B. Drevillon, K. Postava, D. Ciprian, J. Pištora, and K. Watanabe, "Effective medium approximation of anisotropic lamellar nanogratings based on Fourier factorization," Opt. Express **14**(8), 3114–3128 (2006).
41. S. Fan, "Sharp asymmetric line shapes in side-coupled waveguide-cavity systems," Appl. Phys. Lett. **80**(6), 908–910 (2002).